

Tubular catalytic micromotors in transition from unidirectional bubble sequences to more complex bidirectional motion

Cite as: Appl. Phys. Lett. **114**, 033701 (2019); <https://doi.org/10.1063/1.5059354>

Submitted: 20 September 2018 . Accepted: 04 January 2019 . Published Online: 22 January 2019

S. Naeem, F. Naeem, M. Manjare, F. Liao, V. A. Bolaños Quiñones, G. S. Huang , Y. Li , J. Zhang, A. A. Solovev , and Y. F. Mei 



View Online



Export Citation



CrossMark

ARTICLES YOU MAY BE INTERESTED IN

[Nonvolatile voltage controlled molecular spin state switching](#)

Applied Physics Letters **114**, 032901 (2019); <https://doi.org/10.1063/1.5054909>

[Comparing the anomalous Hall effect and the magneto-optical Kerr effect through antiferromagnetic phase transitions in \$Mn_3Sn\$](#)

Applied Physics Letters **114**, 032401 (2019); <https://doi.org/10.1063/1.5066557>

[Topological insulator \$Bi_2Se_3\$ films on rare earth iron garnets and their high-quality interfaces](#)

Applied Physics Letters **114**, 031601 (2019); <https://doi.org/10.1063/1.5054329>



Measure Ready
M91 FastHall™ Controller

A revolutionary new instrument
for complete Hall analysis

 Lake Shore
CRYOTRONICS

Tubular catalytic micromotors in transition from unidirectional bubble sequences to more complex bidirectional motion

Cite as: Appl. Phys. Lett. **114**, 033701 (2019); doi: [10.1063/1.5059354](https://doi.org/10.1063/1.5059354)

Submitted: 20 September 2018 · Accepted: 04 January 2019 · Published Online: 22 January 2019



View Online



Export Citation



CrossMark

S. Naeem,^{1,2} F. Naeem,^{1,2} M. Manjare,¹ F. Liao,³ V. A. Bolaños Quiñones,¹ G. S. Huang,¹  Y. Li,⁴  J. Zhang,⁵ A. A. Solovev,^{1,a)}  and Y. F. Mei^{1,a)} 

AFFILIATIONS

¹ Department of Materials Science, Fudan University, 220 Handan Road, Shanghai 200433, People's Republic of China

² State Key Laboratory for Modification of Chemical Fibers and Polymer Material Science and Engineering, Donghua University, Shanghai 201620, People's Republic of China

³ State Key Laboratory of ASIC and System, School of Microelectronics, Fudan University, Shanghai 200433, People's Republic of China

⁴ Center for Phononics and Thermal Energy Science, School of Physics Science and Engineering, Tongji University, Shanghai 200092, People's Republic of China

⁵ College of Science, Donghua University, Shanghai 201620, People's Republic of China

^{a)} Authors to whom correspondence should be addressed: solovevlab@gmail.com and yfm@fudan.edu.cn

ABSTRACT

The generation of oxygen microbubbles in catalytic microtubes has attracted tremendous attention towards the exploration of unidirectional and overloaded bubble ejection regimes, leading to simple and more complex motions of micromotors. While it is widely believed that a bubble's frequency in a unidirectional regime (i.e., a bubble ejected from a single tubular opening) is random, this study shall demonstrate that periodic oxygen bubble frequencies and sequences can be experimentally controlled using various concentrations of hydrogen peroxide fuel and surfactants. When released from a substrate, unidirectional micromotors self-propel in straight, circular, and helical trajectories, leading to a class of well-predictable or simple micromachines. Under overloaded conditions, micromotors generate bubbles at both tubular openings, which influence the trajectories of micromotor motion strongly. A one-dimensional reaction-diffusion equation is formulated to explain the possible mechanisms of mass transport in microtubes and the transition from the unidirectional to the overloaded regime of micromotors.

Published under license by AIP Publishing. <https://doi.org/10.1063/1.5059354>

Man-made nano-/micro-motors (NMs) consist of autonomous self-propelled nano-/micro-particles of different shapes, including nano-/micro-rods,^{1,2} tubes,^{3–5} and spheres.⁶ NMs are at the cross-border of the recently emerging fields of chemomechanical systems⁷ and bioinspired chemistry in motion,⁸ where novel functions of dynamic nano-/micro-machines are explored, identified, and utilized.^{9–12} NMs can ultimately lead to breakthrough applications in clean energy generation,¹³ cargo payload delivery,¹⁴ biosensing in motion,¹⁵ and biomedical operations.¹⁶ Tubular catalytic micromotors are one of the fastest autonomous micromachines, which are based on efficient nucleation, growth, and recoil of microbubbles.^{17,18} Mei's group developed a model that predicts the linear speeds of tubular

microjets in a unidirectional bubble recoil regime, where the velocities of NMs are linearly proportional to the H₂O₂ concentration, the microtube diameter, the microtube length, and the bubble size.¹⁹ Zhao and co-workers described a one-dimensional mass transport model based on the reaction-diffusion that predicts the O₂ flux, the bubble frequency, the average microjet speeds from the geometrical parameters (i.e., tube diameter and length), and the concentration of H₂O₂ molecules in the solution.²⁰ Gallino *et al.* showed the chemically diffusive, hydrodynamic models of bubble-propelled micromotors and outlined the interesting perspectives of interacting microbubbles in the microcavity.²¹ In biology, despite a simple cylindrical shape, chemotactic bacteria swim in random walks by

alternating tumbles and runs, which helps to obtain a temporal “memory” for the detection of spatial gradients.²² To date, only a few researchers have addressed the problem of how to discover more complex nano-/micro-machines.²³ It is known that the conical shape of tubular micromotors governs the unidirectional recoil of bubbles²⁴ and that the transition to an overloaded regime typically takes place at higher fuel concentrations. The group of Fomin, Misra, and Schmidt has developed a numerical time-resolved model for predicting the transition of tubular micromotors from a unidirectional to an overloaded regime.²⁵ In this study, we shall discuss the tubular micromotors with different lengths generating O₂ microbubbles in unidirectional and overloaded regimes, which have an important influence on the motion of micromotors.

Tubular catalytic micromotors are fabricated using an established experimental procedure (see [supplementary material](#)).³ After fabrication, the tubular catalytic Ti/Cr/Pt micromotors integrated on the silicon substrate were then immersed in an aqueous H₂O₂ fuel solution added with a commercial dish Walch soap (surface tension measurement in the [supplementary material](#)).²⁶ Hydrogen peroxide was decomposed, using catalytic tubular microcavities, into water and oxygen bubbles according to the following reaction: $2\text{H}_2\text{O}_2 \rightarrow 2\text{H}_2\text{O} + \text{O}_2$. [Figures 1\(a\)–I\(h\)](#)

show the schematic and optical microscopy images of an individual 125 μm long microtube generating periodic sequences of O₂ microbubbles (1–8) in a unidirectional regime from one tubular opening (video 1, [supplementary material](#)). [Figure 1\(i\)](#) presents the typical helical, circular, and straight trajectories of micromotors driven by a unidirectional recoil of O₂ bubbles. Swimming micromotors were then tested in an overloaded regime located in mixtures of (i) H₂O₂ with soap to stabilize bubbles and (ii) H₂O₂ with propylene carbonate (PC) to reduce the lifetime of bubbles. At a higher concentration of hydrogen peroxide fuel (H₂O₂ = 20% v/v in soap), transition to the overloaded regime occurred [[supplementary material](#) video 2; [Fig. 1\(j\), left](#)]. In the mixture of peroxide and soap, the micromotor underwent a circular motion and then switched to a rotational trajectory. In the H₂O₂ PC fuel, the O₂ bubbles broke in tens of microseconds, allowing the avoidance of subsequent collisions between the ejected bubbles and self-propelled micromotors. [Figure 1\(j\), right](#) shows the back-and-forth motion of an individual micromotor in the H₂O₂ PC fuel mixture. Such overloaded regimes can have a pronounced influence on the transition of catalytic micromotors to more complex dynamics.

Focusing on microtubes integrated on-chip assists with the assessment of individual micromotors under different chemical

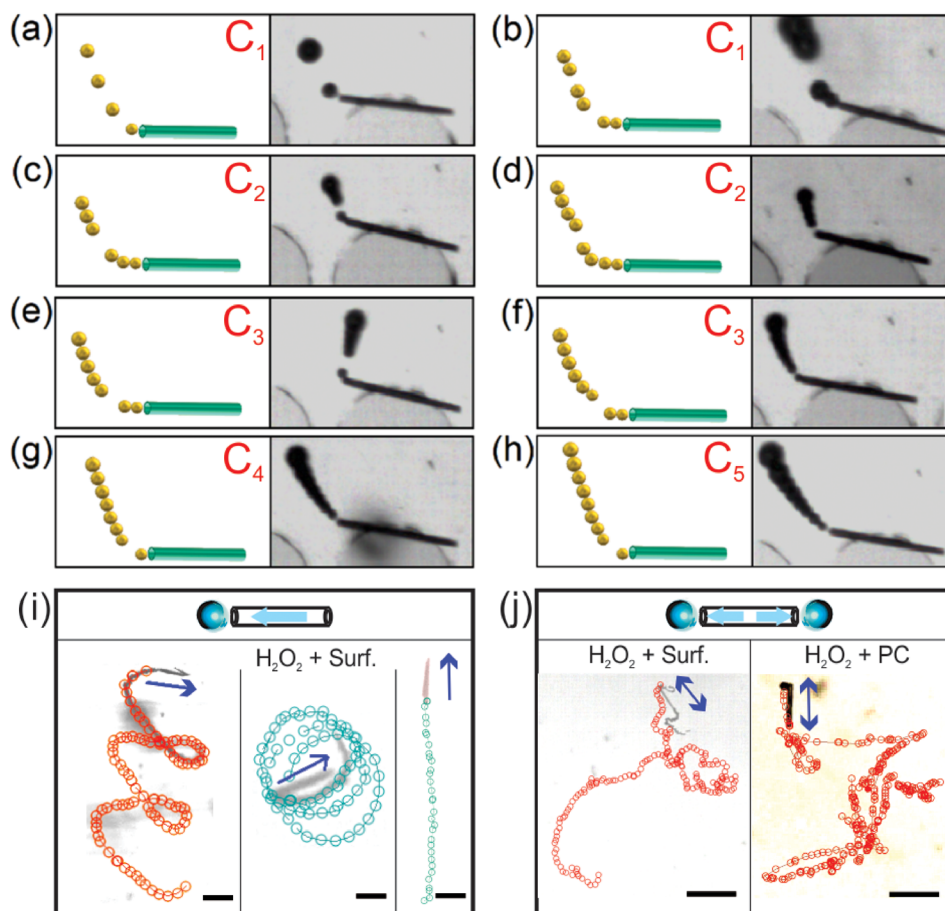


FIG. 1. Generation of periodic microbubble sequences from an individual 125 μm long catalytic microtube integrated on a silicon substrate. (a)–(h) The sketch and optical microscopy images of the corresponding microtube ejecting microbubbles with different fuel compositions: single bubble C₁ (S = 16% v/v, H₂O₂ 1% v/v) and multiple sequences of bubbles: C₂ (S = 32% v/v, H₂O₂ = 0.125%), C₃ (S = 32% v/v, H₂O₂ = 0.25%), C₄ (S = 32% v/v, H₂O₂ = 0.5%), and C₅ (S = 32% v/v, H₂O₂ = 1%). (i) Tracked trajectories in a unidirectional regime of helical, circular, and straight motion tubular micromotors. The scale bar is 50 μm. (j) Optical microscopy image of an individual swimming overloaded Ti/Cr/Pt micromotor in the mixture of dish soap (32% v/v) and H₂O₂ (21% v/v), left image. Initially, a rotational motion was observed followed by transition to rotational motion. The time interval was 1 s. The tracked trajectory of the swimming overloaded micromotor in a mixture of hydrogen peroxide and propylene carbonate (20% v/v H₂O₂ in propylene carbonate) is shown. The blue arrows indicate the direction of micromotor motion. The scale bar is 70 μm.

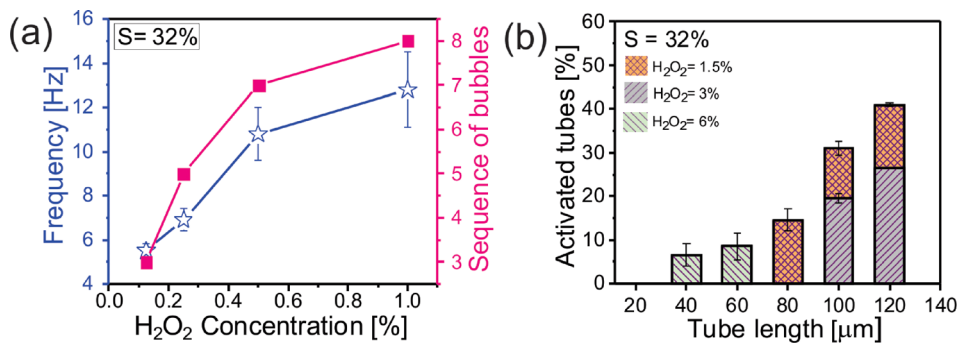


FIG. 2. Characterization of Ti/Cr/Pt microtubes on-chip. (a) The average frequency and sequences of bubbles observed in different concentrations of H₂O₂ (0.125, 0.25, 0.5, and 1% v/v) and at a constant soap concentration of 32% v/v. (b) The population of activated micropump sequences on a chip analysis at different H₂O₂ concentrations in 1.5% v/v H₂O₂ (crosshatching line region), 3% v/v H₂O₂ (right tilted hatched region), and 6% v/v H₂O₂ (left tilted hatched region).

conditions. Figure 2(a) indicates the bubble frequencies and sequences of a 125 μm long microtube, immersed in different H₂O₂ concentrations of 0.125, 0.25, 0.5, and 1% v/v, while keeping a constant dish soap concentration, $S = 32\%$ v/v. Error bars were calculated for each point as a standard deviation of 30 ejected bubbles. Interestingly, a maximum number of eight ejected bubbles in sequence was reached at a given H₂O₂ (1% v/v) concentration that can indicate the limitation of physical space for bubbles in a 125 μm long microtube. It is known that different tubes have slightly different bubble nucleation energy barriers, which are particularly visible at low H₂O₂ fuel concentrations. As a result, depending on the conditions, if one fraction of tubes remains inactive, the other fraction ejects single or multiple O₂ bubbles on the same chip. Figure 2(b) shows the statistical data for activated tubes (from 20 to 120 μm) in 1.5, 3, and 6% v/v H₂O₂, respectively. They correlate favorably with previous reports about catalytic tubular micropumps.^{18,27} The filled-area graph displays bubble sequences observed in 1.5% v/v H₂O₂ (crosshatching line region), 3% v/v H₂O₂ (right tilted hatched region), and 6% v/v H₂O₂ (left tilted hatched region) for activated micropumps.

To better understand the origin of bubble sequences in the microtubular cavity, a semi-transparent Ti/Cr/Pt microtube was fabricated with dimensions of 50 μm in length and 9.5 μm in diameter, which consisted of approximately two rolled-up layers of a metallic nanomembrane. Nucleation, growth, and ejection of O₂ bubbles were clearly observed in the self-propelled catalytic microtube, as shown in Fig. 3(a). During a time period of 100 ms (t_1 – t_4), bubbles in the sequence (N 1, 2, 3, 4) changed their average diameters from (8, 6, 6, 5.8 μm, t_1) to (10.2, 7.8, 8.2, 10.8 μm, t_4), respectively. The observed bubble sequences can be attributed to the difference between the bubble growth time required to reach the critical bubble ejection size (tens of ms) and the bubble recoil time (less than 10 ms). O₂ bubbles located near the tubular openings could reach the ejection diameter faster, while bubbles located in the middle of the catalytic microtube would require more time to reach the critical recoil radius, due to the limited supply of hydrogen peroxide fuel by diffusion. At the same time, bubbles ejected from the tubular opening induced fluid pumping and bubbles remaining in the tube moved closer to the opening. Figure 3(b) shows the results of bubbles ejecting in unidirectional sequences from self-propelled Ti/Cr/Pt microtubes with different lengths (20–120 μm long) at a constant soap concentration ($S = 32\%$ v/v)

and at different hydrogen peroxide (10, 13, 14% v/v) concentrations. At first, self-propelled microtubes were tested in 10% v/v H₂O₂, where bubbles recoiled in a single mode starting from the 80 μm tubular length (see the upper graph, red curve). We show

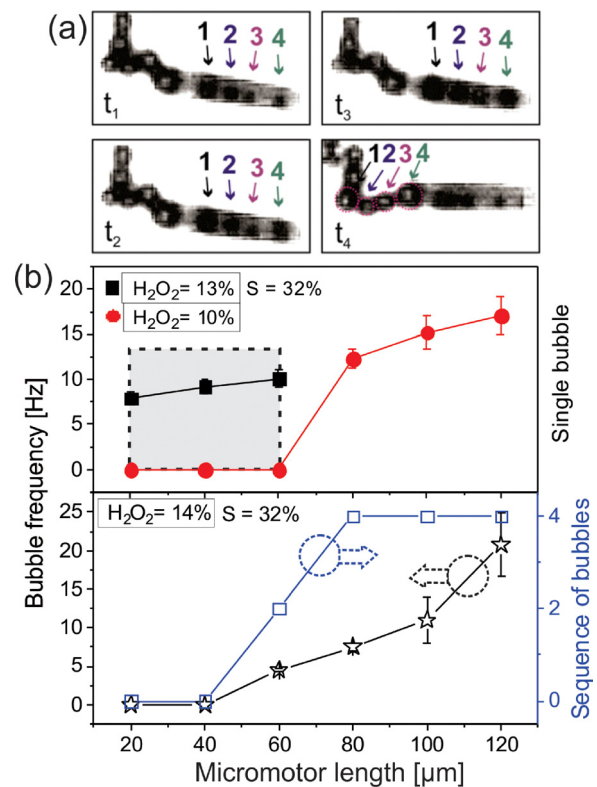


FIG. 3. Analysis of bubble sequences ejected from an individual swimming transparent microtube and bubble sequences of self-propelled microtubes with different lengths. (a) Characterization of bubble evolution and recoil from transparent Ti/Cr/Pt microtubes where individual oxygen microbubbles in a sequence are indicated by numbers (1–4) and colored arrows. (b) Average frequencies and sequences of O₂ bubbles observed in different concentrations of hydrogen peroxide (10, 13, and 14% v/v) and at a constant soap concentration, 32% v/v. At 10% v/v H₂O₂, a single bubble recoil is observed, upper graph (inset shows how increasing H₂O₂ fuel to 13% v/v activates shorter 20, 40, and 60 μm tubes). A further increase in the fuel concentration to 14% v/v H₂O₂ leads to the appearance of bubble sequences (lower graph).

that shorter micromotors (20, 40, and 60 μm) could also be activated and generate single bubbles at 13% v/v H_2O_2 (upper graph, black curve). Sequences of bubbles (2, 4) for longer tubes from 60 to 120 μm were observed at a higher (14% v/v) H_2O_2 fuel concentration (lower graph) with the same soap concentration (32% v/v). For shorter tubes (20 and 40 μm), sequences of bubbles (2) were observed at 17 and 16.5% v/v H_2O_2 , with the frequencies of 6.2 and 6.7 Hz, respectively.

Figure 4(a) clearly shows three regions of on-chip integrated micromotors with different lengths (20–120 μm), which have (i) inactive, (ii) unidirectional, and (iii) overloaded bubble recoil regimes. The substrate can have a significant influence on the nucleation of oxygen bubbles, and the bubble frequencies of microtubes integrated on-chip can be different from free-swimming micromotors.²⁸ In this study, the comparison between free-swimming micromotors and on-chip analysis for both uni- and bi-directional is given in the [supplementary material](#). A theoretical model is considered to better understand unidirectional and overloaded bubble recoil. Previously, Manjare and co-authors formulated a one-dimensional reaction diffusion

equation to describe the mass transport and the reaction in a tubular microjet.²⁰ The position of the maximum, at which the concentration of O_2 is maximum, can be given by

$$x_{\max} = \frac{1}{\beta} \sinh^{-1} \left(\frac{1}{\beta L} (1 - \cosh(\beta L)) \right) + \frac{L}{2}, \quad (1)$$

where $\beta = \left(\frac{2K}{D_{\text{H}_2\text{O}_2} R} \right)^{1/2}$, K is the reaction constant, $D_{\text{H}_2\text{O}_2} = 1.43 \times 10^{-9} \text{ m}^2 \text{ s}^{-1}$ is the diffusion constant of hydrogen peroxide, R is the radius of the tube, and L is the length of the tube. The reaction constant rate was previously calculated by Paxton, $K = 6.83 \times 10^{-7} \text{ m s}^{-1}$.¹ Figure 4(b) plots the x_{\max} versus L for a different R . As shown in Fig. 4(b), the location of maximum oxygen generation occurred towards the non-bubbling end of the tube, but close to midway inside the tube. The trend also shows that, as the length of the tube increased, the position of x_{\max} shifted closer to the non-bubbling end of the tube, since it would take longer for H_2O_2 to diffuse along the tube. This explains that oxygen production is not symmetric along the long axis of the tube. Previously, Manjare *et al.* assumed that the concentration of H_2O_2 was maximum at one end of a microtube, zero at the other end, and vice versa for the O_2 concentration. However, different conditions are applied to our study, and a reasonable assumption can be made in the steady condition (unidirectional): all of the oxygen generated inside the motor is utilized in the formation of bubbles. The equation for oxygen generation rate at a given concentration can be used.²⁰ To analyze the equation further, the effective L in our case is shorter. For example, if a bubble is initially formed at the location $x = L/2$, then at $L/2$, the concentration of H_2O_2 is zero and all of the oxygen generated between $x = 0$ and $x = L/2$ (according to the diffusion plot), is subject to the formation of bubbles. For longer tubes, the oxygen has to travel a longer relative distance towards the far end, where O_2 bubbles eject or burst. Increasing H_2O_2 concentrations produce a rich environment for the nucleation of multiple interactive bubbles, and at higher fuel concentrations, the O_2 bubbles come out from both ends. By substituting the geometrical parameters of the tube, concentrations of H_2O_2 fuel in unidirectional and overloaded regimes and the beta coefficient defined above, the theoretical value of the total mass of O_2 produced can be estimated.²⁰ The same order of magnitude of generated O_2 and a close consistency between our experimental and calculated results are achieved. The experimentally measured values on the order of 10^{-13} – $10^{-14} \text{ kg s}^{-1}$ dictate that there is large amount of oxygen generated inside the tube. This leads to the sequence of bubbles and subsequently to an overloaded regime, since the O_2 concentration is at maximum near the non-bubbling end after the oversaturation bubbles start to appear at the previously non-bubbling end.

In summary, sequences of microbubbles generated by tubular micromotors in a unidirectional regime are reported in a mixture of hydrogen peroxide and high concentrations of a dish soap. A one-dimensional reaction-diffusion equation was used to describe gas generation in microtubes. When released from the substrate, the unidirectional micromotors navigated in predictable straight, circular, or helical trajectories and thus, in our opinion, can be related to the class of simple micromachines.

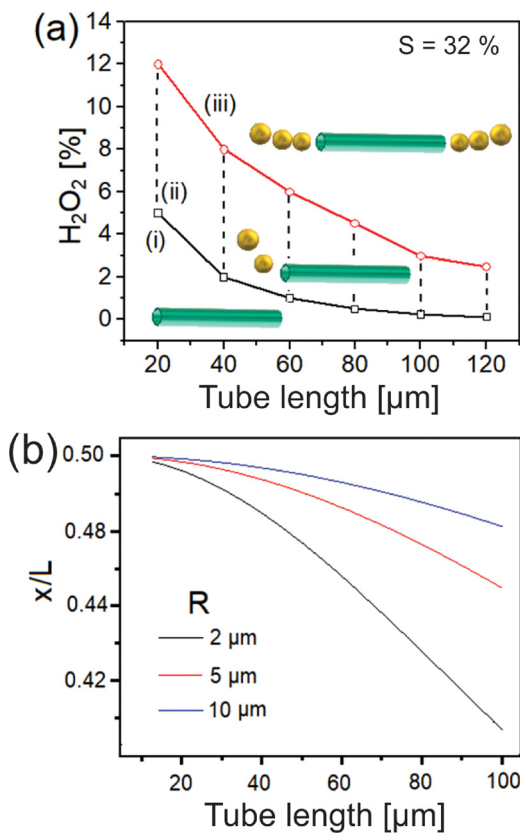


FIG. 4. Analyses of micromotors in unidirectional and overloaded regimes. (a) On-chip Ti/Cr/Pt microtubes with lengths from 20 μm to 120 μm generated bubbles at one and both tubular openings in different concentrations of hydrogen peroxide and at a constant concentration of surfactant (32% v/v). (b) Modelling of the bubble nucleation point, depending on the aspect ratio of the tubular micromotor, for the maximum concentration of oxygen, versus L for different radii.

The dynamics of micromotors under overloaded conditions, where switchable trajectories of motion and bidirectional motilities were observed, are not yet fully understood—more research studies must be undertaken. It will be interesting to study how selective surfactants^{29,30} can influence the generation of bubbles and motion. Overloaded micromotors can be fundamentally important to explore more complex micromachines, which can potentially serve as models of chemotactic bacteria swimming in tumbles and runs.

See [supplementary material](#) for details about fabrication procedure, surface tension measurements, and comparison between fuel concentrations required for unidirectional and overloaded regimes.

A.A.S. is grateful for the financial support from the young “1000 talent” plan. The authors also acknowledge financial support from the Natural Science Foundation of China (Grant Nos. 51475093 and 51850410502). Y.F.M. acknowledges the Changjiang Young Scholars Program of China.

REFERENCES

- ¹W. F. Paxton, K. C. Kistler, C. C. Olmeda, A. Sen, S. K. S. Angelo, Y. Cao, T. E. Mallouk, P. E. Lammert, and V. H. Crespi, *J. Am. Chem. Soc.* **126**, 13424 (2004).
- ²G. A. Ozin, I. Manners, S. Fournier-Bidoz, and A. Arsenaault, *Adv. Mater.* **17**, 3011 (2005).
- ³A. A. Solovev, Y. F. Mei, E. Bermudez Urena, G. S. Huang, and O. G. Schmidt, *Small* **5**, 1688 (2009).
- ⁴Y. Mei, G. Huang, A. A. Solovev, E. Bermudez Urena, I. Moench, F. Ding, T. Reindl, R. K. Y. Fu, P. K. Chu, and O. G. Schmidt, *Adv. Mater.* **20**, 4085 (2008).
- ⁵J. Li, I. Rozen, and J. Wang, *ACS Nano* **10**, 5619 (2016).
- ⁶J. Gibbs and Y. Zhao, *Front. Mater. Sci.* **5**, 25 (2011).
- ⁷J. S. Randhawa, K. E. Laflin, N. Seelam, and D. H. Gracias, *Adv. Funct. Mater.* **21**, 2395 (2011).
- ⁸J. Zhang, E. Luijten, B. A. Grzybowski, and S. Granick, *Chem. Soc. Rev.* **46**, 5551 (2017).
- ⁹H. Ning, Y. Zhang, H. Zhu, A. Ingham, G. S. Huang, Y. F. Mei, and A. A. Solovev, *Micromachines* **9**, 75 (2018).
- ¹⁰H. Wang and M. Pumera, *Chem. Rev.* **115**, 8704 (2015).
- ¹¹P. H. Colberg and R. Kapral, *EPL* **106**, 30004 (2014).
- ¹²K. K. Dey, F. Y. Pong, J. Breffke, R. Pavlick, E. Hatzakis, C. Pacheco, and A. Sen, *Angew. Chem. Int. Ed.* **55**, 1113 (2016).
- ¹³V. V. Singh, F. Soto, K. Kaufmann, and J. Wang, *Angew. Chem. Int. Ed.* **54**, 6896 (2015).
- ¹⁴D. Patra, S. Sengupta, W. T. Duan, H. Zhang, R. Pavlick, and A. Sen, *Nanoscale* **5**, 1273 (2013).
- ¹⁵B. Esteban-Fernández de Ávila, A. Martín, F. Soto, M. A. Lopez-Ramirez, S. Campuzano, G. M. Vásquez-Machado, W. Gao, L. Zhang, and J. Wang, *ACS Nano* **9**, 6756 (2015).
- ¹⁶Y. Tu, F. Peng, A. A. M. Andre, Y. Men, M. Srinivas, and D. A. Wilson, *ACS Nano* **11**, 1957 (2017).
- ¹⁷L. Liu, T. Bai, Q. Chi, Z. Wang, S. Xu, Q. Liu, and Q. Wang, *Micromachines* **8**, 267 (2017).
- ¹⁸A. A. Solovev, S. Sanchez, Y. Mei, and O. G. Schmidt, *Phys. Chem. Chem. Phys.* **13**, 10131 (2011).
- ¹⁹J. Li, G. Huang, M. Ye, M. Li, R. Liu, and Y. F. Mei, *Nanoscale* **3**, 5083 (2011).
- ²⁰M. Manjare, B. Yang, and Y. P. Zhao, *J. Phys. Chem. C* **117**, 4657 (2013).
- ²¹G. Gallino, F. Gallaire, E. Lauga, and S. Michelin, *Adv. Funct. Mater.* **28**, 1800686 (2018).
- ²²H. C. Berg, *Phys. Today* **53**(1), 24 (2000).
- ²³B. Bensaude-Vincent and X. Guchet, *Techné: Res. Philos. Technol.* **11**, 71 (2007).
- ²⁴V. M. Fomin, M. Hippler, V. Magdanz, S. Sanchez, and O. G. Schmidt, *IEEE Trans. Rob.* **30**, 40 (2014).
- ²⁵A. Klingner, I. S. M. Khalil, V. Magdanz, V. M. Fomins, O. G. Schmidt, and S. Misra, *J. Phys. Chem. C* **121**, 14854 (2017).
- ²⁶Commercial dish soap, Walch brand: fatty alcohol polyoxyethylene ether sodium sulfate 7%, cocamidopropyl betaine 7%, alkyl glycoside 2%, polyquaternium 0.1%, fatty glyceride 1.0%, humectant 3%, mixedplantextracts 1%, ethylenediaminetetraacetic acid tetrasodium salt 1%, sodium chloride 0.5%, citric acid 0.1%, jojoba oil 0.05%, 1,2-pentanediol 0.5%, essence 0.2%, water 76.55%.
- ²⁷A. A. Solovev, S. Sanchez, M. Pumera, Y. F. Mei, and O. G. Schmidt, *Adv. Funct. Mater.* **20**, 15 (2010).
- ²⁸A. A. Solovev, E. J. Smith, C. C. Bof Bufon, S. Sanchez, and O. G. Schmidt, *Angew. Chem. Int. Ed.* **50**, 10875 (2011).
- ²⁹H. Wang, G. Zhao, and M. Pumera, *J. Phys. Chem. C* **118**, 5268 (2014).
- ³⁰J. Simmchen, V. Magdanz, S. Sanchez, S. Chokmaviroj, D. Ruiz-Molina, A. Baezaand, and O. G. Schmidt, *RSC Adv.* **4**, 20334 (2014).